Research article

Exploring differential pressure-induced hydraulic flows in pilot-scale Electrodialysis with Bipolar Membranes

Antonia Filingeri [ID], Andrea Culcasi *[ID], Marcantonio Nanfara, Calogero Cassaro, Alessandro Tamburini, Giorgio Micale, Andrea Cipollina

Dipartimento di Ingegneria, Università degli studi di Palermo, Viale delle Scienze ed. 6, 90128 Palermo, Italy

ABSTRACT

Electrodialysis with Bipolar Membranes (EDBM) is an electro-membrane process that produces acid and base from saline solutions using electricity. In previous research, this technology has predominantly been explored at the laboratory scale, with very few examples at the pilot scale. This study investigated, for the first time, how differential pressures applied between the EDBM channels affect its performance, utilizing a semi-industrial scale pilot — the largest ever studied in the literature. For this, inlet pressures from 0.5 to 1.5 barg were applied in the EDBM channels. Results were compared in terms of volume variation, product purities and key performance indicators, such as Current Efficiency (CE) and Specific Energy Consumption (SEC).

Results indicate that changing the pressure between the channels induces a volumetric flow between compartments, which impacts the EDBM's performance. Specifically, the SEC ranged from 1.20 to 1.58 kWh kg_{NaOH}^{-1}, considering the energy required for both electricity and pumping at base concentration of ~0.66 mol L^{-1}. Notably, SEC values were 24% lower than the reference case study when operating with the identified best set of pressures. Under similar conditions, the CE varied between 64 % and 86 %, depending on the pressure applied between the channels.

Moreover, using this set of pressures, acid and base product purities remained above 90%.

This study advances pilot-scale EDBM process intensification, highlighting its potential for reduced energy consumption, increased sustainability, and industrial competitiveness.

1. Introduction

Industrial sustainability is a key challenge in the context of present climate change issues. However, this goal is currently unfeasible using conventional technologies due to their high energy consumption and dependence on critical raw materials (CRMs), as identified by the European Commission (Blengini et al., 2020). Two notable examples of this issue are the industrial production of HCl and NaOH. Hydrochloric acid is typically concentrated via the Pressure Swing Distillation process (Farsi et al., 2019), which results in an aqueous solution with a concentration ranging between 34% and 36% by weight. On the other hand, sodium hydroxide is produced in the form of solid pellets or powder through the chlor-alkali process (Lerch et al., 2024). Producing acids and bases at such high concentrations has several drawbacks. Firstly, their handling presents safety risks. Additionally, the risks extend to their transport from the production site to the place of use, as potential leakage can damage human health and the environment. Moreover, these high-concentration acid and alkaline products are rarely used in this form; instead, they often need to be appropriately diluted to reach the necessary concentrations for the processes they are involved in. Dilution, however, is a form of energy inefficiency, leading to energy loss in the form of heat. For example, producing NaOH in pellets or powder has a high energy cost, amounting to 2.8 kWh kg^{-1} of NaOH produced (Brinkmann et al., 2014). Additionally, the chlor-alkali process produces both NaOH and gaseous Cl_2. Problematically, there is a supply-demand imbalance between NaOH and Cl_2 in the chlor-alkali process, as the production of these two chemicals is not well aligned with the end-user demand. While NaOH is often the more desirable product, Cl_2 is mainly used in the production of PVC, and this fact leads to an oversupply that creates challenges for sustainable industrial development (Wang et al., 2024).

In this context, an alternative and more efficient way to produce

---

* Corresponding author.
E-mail address: andrea.culcasi@unipa.it (A. Culcasi).

these industrial reactants is Electrodialysis with Bipolar Membranes (EDBM). EDBM is an electro-membrane process that, with inputs of freshwater, salty solution, and electricity, can produce an acidic solution, an alkaline solution, and a desalinated stream (Culcasi et al., 2022a). Therefore, EDBM can concurrently produce HCl and NaOH solutions at the desired concentrations, thus eliminating the need to waste energy in the dilution/concentration process and minimizing the carbon footprint. A representative diagram of the EDBM technology describing its working principles is shown in Fig. 1.

The core of the EDBM unit is the stack, which consists of a pile of repetitive units called triplets containing membranes and spacers. In a triplet, there are three different types of ion-exchange membranes, namely anionic (AEM), cationic (CEM), and bipolar (BPM), and three spacers interposed between the membranes to form the space through which the electrolyte solutions flow. Each triplet includes three different channels: one acidic, one alkaline, and one saline. The bipolar membrane is formed of two layers, one cationic and one anionic, stacked together to form a single membrane (Pärnamäe et al., 2021). The pack of triplets is placed between two end-plates containing the electrodes. Next to the electrodes, there is the Electrode Rinse Solution (ERS), which plays an important role in the charge transfer reactions occurring at the electrode surface (Chen et al., 2022a). In line with the semiconductor theory, the EDBM unit acts as a p-n junction in reverse bias mode (Pärnamäe et al., 2020). During operation, an electric field is applied between the two electrodes, and the electrolyte solutions are pumped through the channels. In the interlayer (or transition region) of the bipolar membrane, the water dissociation reaction occurs, thus producing protons and hydroxide ions. At the same time, the saline ions in the salt compartment are forced to move towards the acidic and alkaline compartments, driven by the electric field. This process results in the production of acidic and alkaline solutions and of a desalinated solution stream. EDBM was also investigated for the recovery of total ammoniacal nitrogen (Deng et al., 2021), lithium (Chen et al., 2021), saline wastewater (Chen et al., 2022b), and organic acids (An et al., 2022).

EDBM has been used for the production of acidic and alkaline chemicals in the treatment of waste saline solutions, such as brines from Reverse Osmosis (RO) desalination plants with Minimum Liquid Discharge (MLD) (Bello et al., 2021) or Zero Liquid Discharge (ZLD) strategies (Cassaro et al., 2023). In particular, in the SEArcularMINE treatment chain (SEArcularMINE website), EDBM was used to produce the acidic and alkaline solutions in-situ, and these were then recirculated back to the other process units of the treatment chain (León et al., 2022). Notably, in-situ production offers advantages in terms of both economic cost savings and environmental sustainability (Herrero-Gonzalez et al., 2024).

In the previous literature, EDBM has been studied almost entirely on a small laboratory scale, with active membrane areas below 200 cm^2 and less than 10 triplets (Hussain et al., 2022; Tang et al., 2023; Song et al.,

2021; Ghyselbrecht et al., 2014). Only a few studies were conducted with semi-industrial scale units, comprising two stacks of 20 triplets each in series and a membrane area of 0.16 m^2 (Cassaro et al., 2023). Furthermore, previous research has mainly focused on parametric analyses, varying the applied current or voltage, the saline feed composition, the use of a single salt or multi-ionic solutions, and the feed concentration at fixed composition. Energy consumption and process efficiency variations with different single salts in the feed have also been assessed (Hussain et al., 2023). Recently, the performance of EDBM with Na$_2$SO$_4$ solutions or a mix of Na$_2$SO$_4$ and NaCl has been analyzed to investigate the differences in specific energy consumption (Adiba et al., 2024). In another study, differential ion transport across the membranes was examined by calculating the selectivities and ion transport numbers for multi-ionic saline feeds of KCl, Na$_2$SO$_4$, and NaCl (Filingeri et al., 2023a). Generally, the EDBM process for producing HCl and NaOH has been used with target concentrations below 2.0 mol L^{-1} (León et al., 2022). However, recent studies have achieved concentrations up to 6.2 mol L^{-1} NaOH at a current density of 1000 A m^{-2} with an integrated system of conventional electrodialysis followed by EDBM (Fu et al., 2023). Other studies have focused on varying the ratio of acidic, alkaline, and saline solution volumes (León et al., 2024) and using alternative EDBM layouts where the initial saline solution is fed not only to the salt compartment but also to the acid, base, or both (Filingeri et al., 2024). Another important, though poorly-investigated, phenomenon in the EDBM process is the occurrence of parasitic currents via manifolds (also known as shunt currents or short-cut currents) (Culcasi et al., 2020), as well as thermal dissipation of the unit due to the Joule effect (Peng et al., 2022). In fact, in terms of system optimization (Culcasi et al., 2023) and techno-economic analysis studies, it appears that the energy cost of EDBM largely determines the Operating Expenditures (OPEX) for both EDBM or integrated RO-EDBM systems (Ankoliya et al., 2023).

Additionally, OPEX are generally higher than Capital Expenditures (CAPEX), thus highlighting the importance of minimizing operating costs of EDBM (Virruso et al., 2024), i.e., reducing the plant energy consumption and pumping power.

In this regard, parametric analyses have been carried out by varying the average flow velocity in the channels or the volumetric flow rates of the circulating solutions in the stack (Liu et al., 2024). However, in lab-scale EDBM or similar electro-membrane processes such as conventional Electrodialysis (ED) (Filingeri et al., 2023b) or Reverse Electrodialysis (RED) (Culcasi et al., 2021), the flow velocity is usually varied in all compartments of the electrolyte solutions. Pressure losses in response to variations in flow velocity were examined at both the laboratory-scale (Pawlowski et al., 2014) and pilot-scale (Veerman et al., 2010). However, these studies only focused on the effect of flow velocity on pressure losses and, thus, the power spent on pumping the electrolyte solutions.
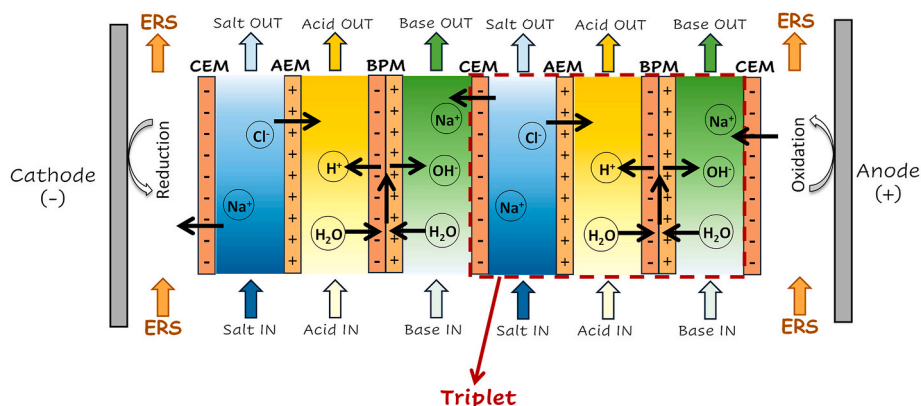

Fig. 1. Schematic representation of the EDBM unit.

Only two works by Tanaka, 2004a, 2004b, dated back 20 years ago, have studied the effect of internal leakage, which is the undesired passage of solution from one compartment to another. This leakage occurs due to pinholes present on the membrane surface or defects such as gaps in the stack assembly caused by poor alignment of membranes and spacers. Importantly, internal leakage is often the result of differential pressure between adjacent compartments. Moreover, in a previous study, the effect of water flow due to osmotic pressure differences between channels was discussed (Wang et al., 2024). However, none of the previous studies addressed the effect of applying differential pressure between the compartments of an EDBM stack. Generally, at the laboratory scale, pressures at the stack inlet are not even monitored. Potential differential pressures arising between adjacent channels could cause variations in water flux through the membranes, either exacerbating or mitigating the effects associated with osmotic and electro-osmotic water transport (Culcasi et al., 2022b).

For the first time, this work explores the presence of differential pressures between adjacent compartments in an EDBM unit affects its performance. To the best of the authors' knowledge, this EDBM unit is the largest ever presented in the literature, highlighting the high industrial relevance of the work. For this purpose, an original experimental campaign was conducted producing acidic and alkaline solutions at concentrations of up to 1.0 mol L^{-1} NaOH and HCl, varying the operating pressures in the three compartments in the range of 0.5–1.5 barg.

2. Material and methods

This section describes the EDBM pilot plant, the tests conducted, and the performance parameters used for post-processing the results.

2.1. Pilot plant description

2.1.1. The EDBM unit

The EDBM unit was supplied by WTS. The unit includes 50 repetitive cells and has a gross area of 1.30×0.71 m^2, with an active membrane area of 1.71 m × 0.19 m in a U-shape. The unit assembles WTS ion-exchange membranes, including anionic AR103N, cationic CR61N, and treated anionic AR103N membranes. Indeed, the bipolar membrane is composed of two layers: the cationic membrane (i.e., CR61N) and the treated anionic membrane (i.e., AR103N treat.). The AR103N treat. membrane differs from the standard AR103N membrane as it contains a catalyst that facilitates the water dissociation reaction on its surface. However, no information is available from the manufacturer or in the literature regarding the AR103N treat. Table 1 reports the properties of the monopolar membranes CR61N and AR103N.

The stack has a total active membrane area of 48 m^2. The spacers are of woven and of polypropylene net with a thickness of 760 μm. The EDBM stack features three compartments (acid, alkaline, and saline) and lacks a separate ERS compartment, as it uses the alkaline solution as the

Table 1

Properties of the CR61N and AR103N membranes used in this work (Filingeri et al., 2023a).

Membrane characteristics	Units	Membrane type	
	–	CEM	AEM
Identification	–	CR61N	AR103N
Cloth type	–	Thin polypropylene non-woven	
Thickness	μm	300	300
Ion exchange	meq dry g^{-1} resin	2.20	2.37
[a]Areal resistance	Ω cm^2	3.6	2.8
Water content	% wet resin	44	39
Permselectivity	%	95	92
Burst strength	psi	95	95

n.a. not available.

[a] Measured in 0.1 N NaCl solution.

ERS. The cathode is made of stainless steel, while the anode is made of platinum-plated titanium. The EDBM unit is placed within a containment basin and connected to the DC power supply through three cables that are welded to their corresponding electrical terminals: positive, negative, and ground. The DC power supply is a high-frequency DC drive device (type AF02, Giussani s.r.l.) with a maximum power of about 18 kW.

2.1.2. Hydraulic circuits and relevant sensors

Three identical hydraulic circuits were constructed for the acid, alkaline, and saline compartments. These circuits include pumps, valves, measurement and control devices, and are housed within an aluminum structure, referred to as the hydraulic cart. Fig. 2 shows a schematic representation of the EDBM plant. The hydraulic cart is equipped with two containment basins at the bottom and one at mid-height to contain any potential leaks during plant operation.

For safety reasons, the cart is closed with PLEXIGLASS panels to contain any splashes of acidic, alkaline, or saline solutions that may occur due to potential leaks or ruptures in the hydraulic circuit. The EDBM unit was operated with an average channel flow velocity ranging from 5 cm s^{-1} to 10 cm s^{-1}, corresponding to a volumetric flow rate range of 25–50 L min^{-1}, guaranteed by three regenerative turbine pumps (TEOREMA PTM®). Each of the three hydraulic circuits is equipped with a cartridge filter (Atlas®) and air venting valves at the highest points. The filter with a mesh of 1 μm prevents channel plugging in the stack. Sampling points are located at the inlet and outlet of the EDBM stack in each hydraulic circuit. Pressure and flow meters (OPTIBAR P 1010 C and OPTIFLUX 4100, respectively, KROHNE®) allow to monitor the EDBM operating conditions. Pressure transducers are positioned near the inlet of the stack's electrolyte solution distributors, just before the cartridge filters. Conductivity and temperature are measured and acquired by inductive conductive and temperature sensors (OPTISENS IND 1000, KROHNE®).

2.1.3. Acquisition and control system

The data acquisition hardware includes a chassis (NI cDAQ-9188) with acquisition and command boards from National Instruments®. The acquisition and control signals are analog (0–10 V or 4–20 mA). The pilot plant is monitored and controlled via LabVIEW user-friendly graphical interface developed for quick operator command action. Proportional-Integral (PI) feedback control logics are used to control the pressures in the three compartments and apply the electric potential (in potentiostatic operation) or the electric current (in galvanostatic operation). Initial gains and time constants for the proportional and integral controllers were derived from empirical correlations and later finetuned.

2.1.4. Electrical circuits

The electrical system consists of three main circuits, AC to the rectifier, AC for the pump, and DC for components such as sensors, protected by various safety elements, including circuit breakers, fuses, and relays, with general shutdown controls via a rotary switch and emergency button.

2.1.5. Solution tanks

The pilot plant is equipped with six IBC-type containers, each with a capacity of 1 m^3, allowing the system to operate under various configurations (Section 2.2). All tanks are externally graduated to monitor the solution levels inside. The solution volume in the reservoirs is monitored during each sampling, approximately every 30 min. All six containers are placed on containment basins.

2.2. Pilot plant operating modes

The EDBM system was operated in batch (closed-loop) mode for acid/base production tests. In the batch tests, the solution was
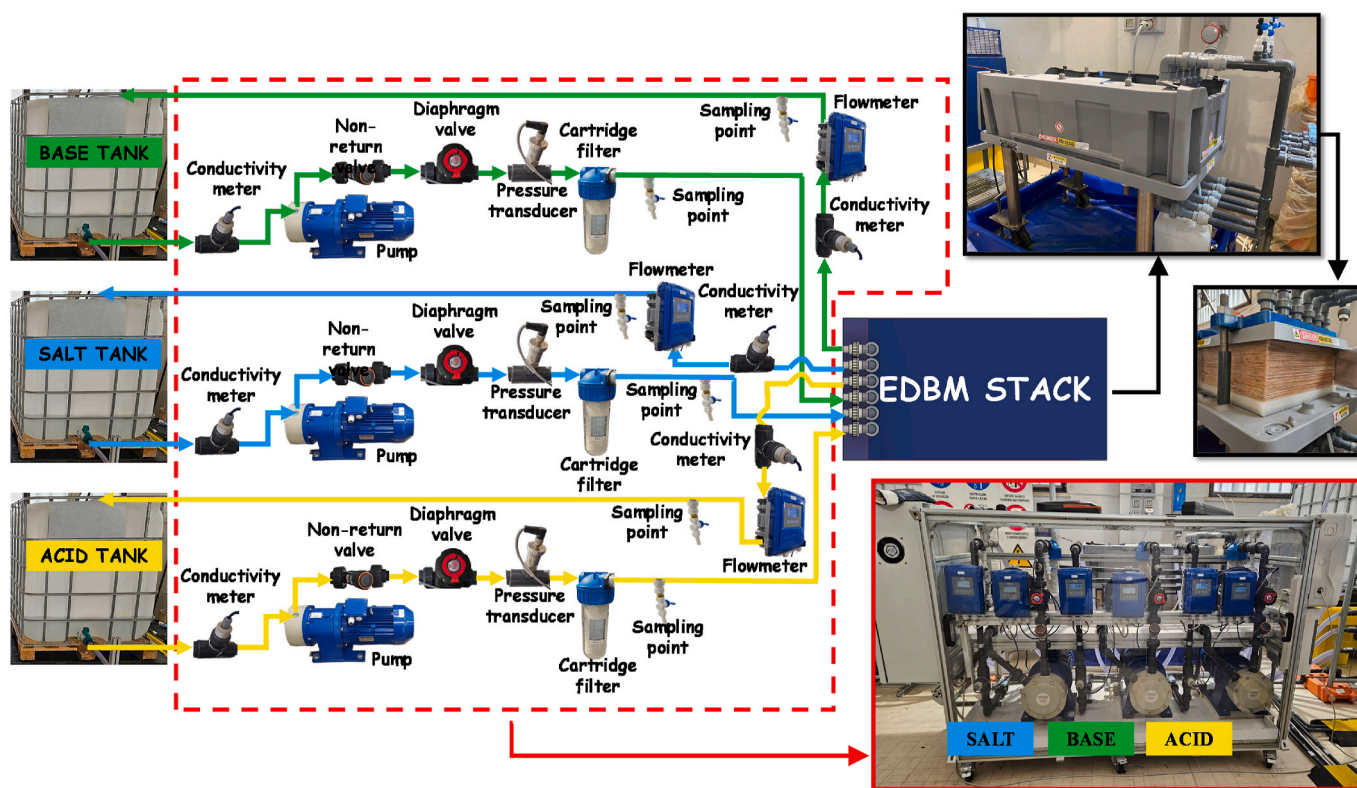
Fig. 2. Simplified diagram of the EDBM plant, including real photos showing the EDBM unit and the pumping station.

recirculated within the same container until the final target concentration of at 1.0 mol L^{-1} NaOH in the base compartment was reached. However, even if the concentration was below 1.0 mol L^{-1}, the test was concluded if a plateau in NaOH concentration was observed or if a duration of the experiments of 360 min was achieved. This concentration target was chosen in order to focus on the in-situ production of chemical solutions of low to medium concentration. This strategy of producing lower-concentration solutions is gaining interest in industry as they can be employed directly by other units in treatment chains as an alternative to use external reagents.

Periodic leakage tests were performed using only softened water for each set of applied pressures (Table 2, Section 2.2) without applying an electric potential to evaluate the extent of possible external and internal leakage.

The inlet pressure to the stack was controlled in the acid, base, and salt compartments, with the volumetric flow rate of the solutions serving as manipulation variable for the pressure controller. Pressures were varied between 0.5 and 1.5 barg in the three compartments to study the effect of differential pressure between channels. The selected pressure range corresponds to the typical nominal flow rates, ensuring appropriate flow characteristics within the spacers.

Table 2 lists the tests conducted and the applied pressures for each channel. It was not possible to carry out the test at 0.5 bar pressure in the base channel because of the accumulation of gas bubbles generated at

the electrodes in the alkaline channels, which led to an increase in electric resistance and process instability.

Between tests, the EDBM unit and the acid, base, and salt compartments conduits were washed with softened water in open-loop mode. The washing phase was carried out for a sufficient duration to reduce the conductivity of the solution in the monitored segment of the hydraulic circuit, from the EDBM outlet to the containers, to a value of 1.1 times the conductivity of the softened water entering the system.

2.3. Preparation of electrolyte solutions

The acidic, alkaline, and saline electrolyte solutions are synthetic and prepared using softened water. Water softening is essential to minimise the presence of calcium and magnesium ions below 10 ppm of CaCO$_3$ equivalent, in order to prevent damage to the membranes. Water hardness was periodically measured using EDTA titrations to ensure that the hardness level consistently remained below the required limit.

NaCl (>99.5% purity, Saline di Volterra s.r.l., Italy) was used to prepare the saline solution at an initial concentration of 1.0 mol L^{-1}. NaOH (technical grade, Inovyn) was used in micro-pearls for the preparation of the base solution. The HCl (ACS Reagent 37%, Honeywell, Fluka) was utilized to prepare the acid solution. Both acid and base solutions were prepared at an initial concentration of 0.05 mol L^{-1} to avoid an excessively low initial concentration that would occur if softened water were used instead. This would otherwise lead to very high channel resistance. During preparation, the solutions were thoroughly mixed using a mechanical stirrer. As already mentioned in Section 2.1, in contrast to the more conventional four-compartment EDBM configuration, only three electrolyte solutions are used in this system (acid, base, and salt), as the base solution also serves as the ERS, flowing through both the base and electrodic channels.

Table 2
List of the experimental tests performed with the EDBM pilot plant.

#Code	P$_a$ [barg]	P$_s$ [barg]	P$_b$ [barg]
P$_{all}$ = 1.0	1.0	1.0	1.0
P$_a$ = 0.5	0.5	1.0	1.0
P$_a$ = 1.5	1.5	1.0	1.0
P$_s$ = 0.5	1.0	0.5	1.0
P$_s$ = 1.5	1.0	1.5	1.0
P$_b$ = 1.5	1.0	1.0	1.5

2.4. Test procedure

At the beginning of the experiment, the desired inlet pressure was set in the three hydraulic circuits, and the solutions were allowed to flow through the circuits for a few minutes to allow the system to stabilise. The initial volumes of the solutions were 250 L for the acid and base, and 500 L for the salt. The electric potential and applied current were recorded using the acquisition and control system, as previously described in Section 2.1. During the initial phase of operation, the Open Circuit Voltage (OCV) was measured using both the acquisition and control system and a portable multimeter, which had been connected to the electrodes of the EDBM unit prior to the test as a cross-check. Once the measured OCV value stabilized, the electric potential was applied.

The tests begin in voltage control mode with the power supply set to 75V. Potentiostatic mode was initially used to prevent excessively high electric potentials, particularly when acid and base concentrations were low. Consequently, the current density increased in the initial phase of the test due to a reduction in resistance caused by the rising concentrations of acid and base. Once a current density of 200 A m^{-2} was reached, the test was switched from potentiostatic to galvanostatic operation. However, if the electric potential required to maintain a current density of 200 A m^{-2} exceeded 75V, as happened in some cases towards the end of the test, the system reverted to potentiostatic mode, operating at the set maximum potential limit of 75V, resulting in a current density lower than 200 A m^{-2}.

During the test, 50 mL samples of the solutions were taken from each compartment approximately every 30 min from the sampling points (see scheme in Fig. 2). These solutions were subsequently subjected to acid-base titration analysis to measure the concentration of H$^+$ and OH$^-$ ions and to chromatographic analyses (Metrohm 882 compact IC plus) to measure the concentrations of the other ions present in the solutions, particularly macro-ions such as Na$^+$ and Cl$^-$. All other relevant variables, such as corresponding voltage/current intensity (depending on the operation mode), volumetric flow rates, pressures, temperature, pH, and conductivity, were extracted from the data recorded by the Labview® software and exported to Excel for data processing.

Periodically, tests were repeated to verify the system's repeatability. Importantly, an average deviation between test and retest below 5% was observed.

2.5. Data processing and performance metrics

The data obtained from the analysis of samples taken during the tests, as well as the sensor data recorded using Labview®, were processed in an Excel spreadsheet.

By analyzing the volume variations in the containers during the tests, it is possible to assess the extent of water flow entering or exiting each of the three compartments. Therefore, the solution flux (J_{sol}, L m^{-2}·h^{-1}) was calculated as follows (Equation (1)):

$$J_{sol} = \frac{V_{sol,t} - V_{sol,0}}{N\,A_m\,\Delta t} \tag{1}$$

where $V_{sol,t}$ and $V_{sol,0}$ are the solution volumes (L) at the generic time t and at the beginning of the test, respectively, N is the number of triplets (−), A_m is the active membrane area (m^2) and Δt is the time interval between the beginning and the generic time t (h) during the tests.

This solution flux is correlated with the water flux related to the osmotic- and electro-osmotic phenomena but also to an additional flux of solution, here named "hydraulic" flux, related to the applied differential pressure between channels. In order to estimate the hydraulic flux (J_{hydr}), two different approaches were utilized.

In the first approach, the test performed at equal pressures (1.0 barg) in the three channels was assumed as a reference test to empirically estimate the water flux related to osmotic- and electro-osmotic phenomena. The hydraulic flux was then calculated by subtracting the water flux estimated during the reference test from the flux obtained in each compartment in the generic test performed by varying the inlet pressures.

The second approach involves the assumption of estimating J_{hydr} (L m^{-2}·h^{-1}) as the difference between the overall solution flux, J_{sol} (L m^{-2}·h^{-1}), and the water flux, J_w (mL m^{-2}·h^{-1}), due to osmotic and electro-osmotic phenomena.

$$J_{hydr} = J_{sol} - \frac{J_w}{1,000} \tag{2}$$

The total water flux, J_w, was estimated from the experimental ionic flux data and the osmotic pressure values, calculated using the PHREEQC software (U.S. Geological Survey, 2017), as follows:

$$J_w = J_{w,os} + J_{w,eo} = k_w \cdot \Delta\pi + \frac{1,000}{\rho_w} \cdot \sum_i M_{H_2O} \cdot n_{H,i} \cdot J_i \tag{3}$$

where $J_{w,os}$ and $J_{w,eo}$ (mL m^{-2}·h^{-1}), are the osmotic and electro-osmotic fluxes, respectively, contributing to the overall water flux. Osmotic flux was calculated using membrane osmotic permeabilities of 7.8 mL m^{-2} h^{-1} bar^{-1} for the CEM and 6.3 mL m^{-2} h^{-1} bar^{-1} for the AEM, as reported by Culcasi et al. (2022b). Hydration numbers were set to 8 for Na$^+$, 6 for Cl$^-$, 8.6 for SO$_4^{2-}$, 6 for K$^+$, 1 for H$^+$, and 1 for OH$^-$, according to reference (Marcus, 2015). M$_{H_2O}$ is the water molecular weight (g mol^{-1}) and ρ_w is the water mass density (g L^{-1}).

The molar flux of the generic ion, i, across the membrane, J_i (mol m^{-2}·h^{-1}), is calculated as:

$$J_i = \frac{\left(V_{sol,t} \cdot C_{i,sol,t} - V_{sol,0} \cdot C_{i,sol,0}\right)}{N\,A_m\,\Delta t} \tag{4}$$

where $C_{i,sol,t}$ and $C_{i,sol,0}$ are the ion concentrations (mol L^{-1}) at the generic time t (h) of the test and at the beginning of the test, respectively.

The osmotic pressure in each compartment, π (in bar), was estimated as:

$$\pi = \varphi \cdot R \cdot T \cdot \sum_i C_{i,sol} \tag{5}$$

where the osmotic coefficient, φ (−), was determined by PHREEQC, R (bar L mol^{-1} K^{-1}) is the gas ideal constant, and T (K) is the temperature.

In both approaches, the resulting hydraulic flux, J_{hydr}, due to the application of differential pressure, was modelled as the product of an average apparent membrane permeability and the driving force, represented by the pressure difference between adjacent channels, as in Equation (6).

$$J_{hydr} = K_{hydr}\,\Delta P \tag{6}$$

where K_{hydr} is the average apparent membrane permeability (L m^{-2} h^{-1} bar) and ΔP (bar) is the differential pressure between adjacent compartments.

Additionally, the main performance metrics of the EDBM unit were calculated. Specifically, the current efficiency (CE, −) is the ratio of the amount of charge effectively converted into OH$^-$ ions to the total charge supplied to the EDBM unit (Equation (7)):

$$CE = \frac{\left(C_{OH^-,t} \cdot V_{base,t} - C_{OH^-,0} \cdot V_{base,0}\right) \cdot z\,F}{N \cdot 3,600 \cdot \int_0^t I\,dt}\,100 \tag{7}$$

where $C_{OH^-,t}$ and $C_{OH^-,0}$ are the OH$^-$ concentrations (mol L^{-1}) while $V_{base,t}$ (L) and $V_{base,0}$ (L) are the base solution volumes at the generic time t and at the beginning of the test respectively, and I (A) is the electric current intensity.

An important productivity index of the EDBM is the specific quantity of NaOH produced during the tests, given by Equation (8):

$$NaOH\ Molar\ flux = \frac{\left(C_{OH^-,t}\cdot V_{base,t} - C_{OH^-,0}\cdot V_{base,0}\right)}{3\cdot A_m\cdot N\cdot \Delta t} \tag{8}$$

The Specific Energy Consumption (SEC_{EDBM}) is the energy consumed by the EDBM unit per kilogram of NaOH produced, given by Equation (9):

$$SEC_{EDBM} = \frac{\int_0^t U\cdot I\ dt}{\left(C_{OH^-,t}\cdot V_{base,t} - C_{OH^-,0}\cdot V_{base,0}\right)\cdot M_{NaOH}} \tag{9}$$

in which U is the electric potential and M_{NaOH} is the NaOH mole mass (g mol^{-1}).

The Specific Energy Consumption associated with the power spent on pumping the electrolyte solutions (SEC_{pump}, kWh kg^{-1}) is given by:

$$SEC_{pump} = \frac{10^5\cdot \Delta t\cdot \sum\limits_{Acid,Base,Salt} \overline{Q}_{sol,EDBM}\Delta \overline{P}_{sol,EDBM}}{\eta_p\cdot M_{NaOH}\cdot \left(C_{OH^-,t}\cdot V_{base,t} - C_{OH^-,0}\cdot V_{base,0}\right)} \tag{10}$$

where $\overline{Q}_{sol,EDBM}$ (m^3 s^{-1}) and $\Delta \overline{P}_{sol,EDBM}$ (bar) are the average volumetric flow rate and the pressure losses of the generic *sol* compartment of the EDBM unit, and η_p is the efficiency of the pumps (assumed equal to 0.75).

The total Specific Energy Consumption (SEC_{tot}) includes the energy consumed by both the EDBM unit and the pumps. This provides a more accurate measure of the actual energy consumption of the plant.

$$SEC_{tot} = SEC_{EDBM} + SEC_{pump} \tag{11}$$

The theoretical Gross Energy Density (GED_{th}, kWh m^{-3}) is the minimum energy required by the process to produce acid/base solutions.

$$GED_{th} = \frac{F}{3.6\cdot 10^3}\cdot \int\limits_{C_{initial}}^{C_{target}} E_{Nernst}\ dC \tag{12}$$

where E_{Nernst} (V) is the electric Nernst potential arising across the monopolar and bipolar membranes, and C is the array of ion concentrations (i.e., H$^+$, OH$^-$, Na$^+$, and Cl$^-$) in the three compartments. The electric Nernst potential (E_{Nernst}) was calculated according to the following formula,

$$E_{Nernst} = \frac{N\cdot R\cdot T}{F}\left(\ln\frac{C_{H^+,acid}}{C_{H^+,BPMint.}} - \ln\frac{C_{OH^-,BPMint.}}{C_{OH^-,base}} + \ln\frac{C_{Na^+,base}}{C_{Na^+,salt}} - \ln\frac{C_{Cl^-,salt}}{C_{Cl^-,acid}}\right) \tag{13}$$

in which $C_{H^+,acid}$ and $C_{H^+,BPM\ int.}$ are the proton concentrations in the acid solution and in the interlayer of the bipolar membrane, $C_{OH^-,BPM\ int.}$ and $C_{OH^-,base}$ are the hydroxide ion concentrations in the interlayer of the bipolar membrane and in the base solution, $C_{Na^+,base}$ and $C_{Na^+,salt}$ are the sodium ion concentrations in base and salt solutions, respectively, and $C_{Cl^-,salt}$ and $C_{Cl^-,acid}$ are the chloride ion concentrations in the salt and acid solutions, respectively.

The EDBM Gross Energy Density (GED_{EDBM}, kWh m^{-3}) is the energy required by the unit for the production of 1 cubic meter of alkaline solution at a specific concentration. It is given by:

$$GED_{EDBM} = \frac{\int_0^t U\cdot I\ dt}{V_{base,t}} \tag{14}$$

The Pump Energy Density (PED, kWh m^{-3}) is the energy required by the pumps for the production of 1 cubic meter of alkaline solution at a specific concentration. It is calculated as:

$$PED = \frac{10^5\cdot \int_0^t \left(\Delta P_{tot,a}Q_{tot,a} + \Delta P_{tot,b}Q_{tot,b} + \Delta P_{tot,s}Q_{tot,s}\right)\ dt}{\eta_p\cdot V_{base,t}} \tag{15}$$

where $\Delta P_{tot,a}$, $\Delta P_{tot,b}$ and $\Delta P_{tot,s}$ are the pressure losses (bar) through the EDBM unit for the three acid, base and salt solutions, respectively, $Q_{tot,a}$,

$Q_{tot,b}$ and $Q_{tot,s}$ are the volumetric flow rates (m^3 h^{-1}) for the acid, base and salt, respectively, and η_p is the pump efficiency (assumed equal to 0.75).

The EDBM energy efficiency (η_{EDBM}, $-$) can be defined as the ratio between the theoretical and the practical energy density.

$$\eta_{EDBM} = \frac{GED_{th}}{GED_{EDBM}} \tag{16}$$

Finally, the total energy efficiency (η_{total}, $-$) can be defined as the ratio between the theoretical and total energy density.

$$\eta_{total} = \frac{GED_{th}}{GED_{EDBM} + PED} \tag{17}$$

3. Results and discussion

In this section, the results are presented and divided into three subsections. First, the analysis of the measured operating variables under the influence of differential pressures is discussed. Next, the effect of differential pressures on the hydraulic flow and apparent permeability is examined. Finally, the purities and key performance indicators of the EDBM unit are presented.

3.1. Analysis of measured operating variables under the effect of differential pressures

Fig. 3 shows the resulting volume profiles of acid, base, and salt over time for all the investigated operating conditions.

Fig. 3 demonstrates that, when a differential pressure applies between the EDBM compartments, a significant change in the volume profiles of the acid and salt appears, with negligible differences in the alkaline solution volume. It should be noted that the tests were conducted under identical operating conditions, except for varying the pressure at the stack inlet. Therefore, the observed variations in the volume profiles are due to the applied differential pressures. Interestingly, the base volume profile (Fig. 3a) remained almost unchanged under the different scenarios investigated, thus suggesting that this solution flux does not occur across the CEMs and the BPMs. It is important to remember that the EDBM stack included only three compartments hosting the electrolyte solutions and thus the electrode compartment contained the same alkaline solution. Therefore, the absence of solution flux (due to the application of differential pressures) across the CEM is advantageous as it minimizes the passage of chloride ions into the anodic channel, thus reducing the risk of chlorine evolution. Conversely, the acid and salt compartments (Fig. 3b and c) exhibited mirrored volume profiles with significant variations when changing the applied pressures, thus again highlighting that the AEM is the only membrane subject to this solution flow.

The effect of differential pressures between adjacent channels has not been previously investigated in the literature for electrodialysis-related systems. Despite this, a partial comparison can be made between the volume profile trends over time obtained in this work and those from our earlier laboratory-scale study (Filingeri et al., 2023a) using the same membranes (see Table 1). In the laboratory-scale study, the operating pressures were not varied, and the pressures measured at the pressure gauges were similar across all compartments. Therefore, these laboratory-scale experimental tests are similar to the $P_{all} = 1$ scenario in the present work. Under these conditions, the results obtained at both the laboratory and pilot scales were qualitatively similar, as both showed a slight increase in the volume of the acidic and alkaline solutions and a concurrent decrease in the saline solution volume. It is widely accepted that osmotic and electro-osmotic flows can occur at different rates across anionic and cationic membranes. Moreover, these flow types are present regardless of the pressure gradient between the channels, as they are not directly dependent on the pressure gradient across the membrane. On the other side, these osmotic and
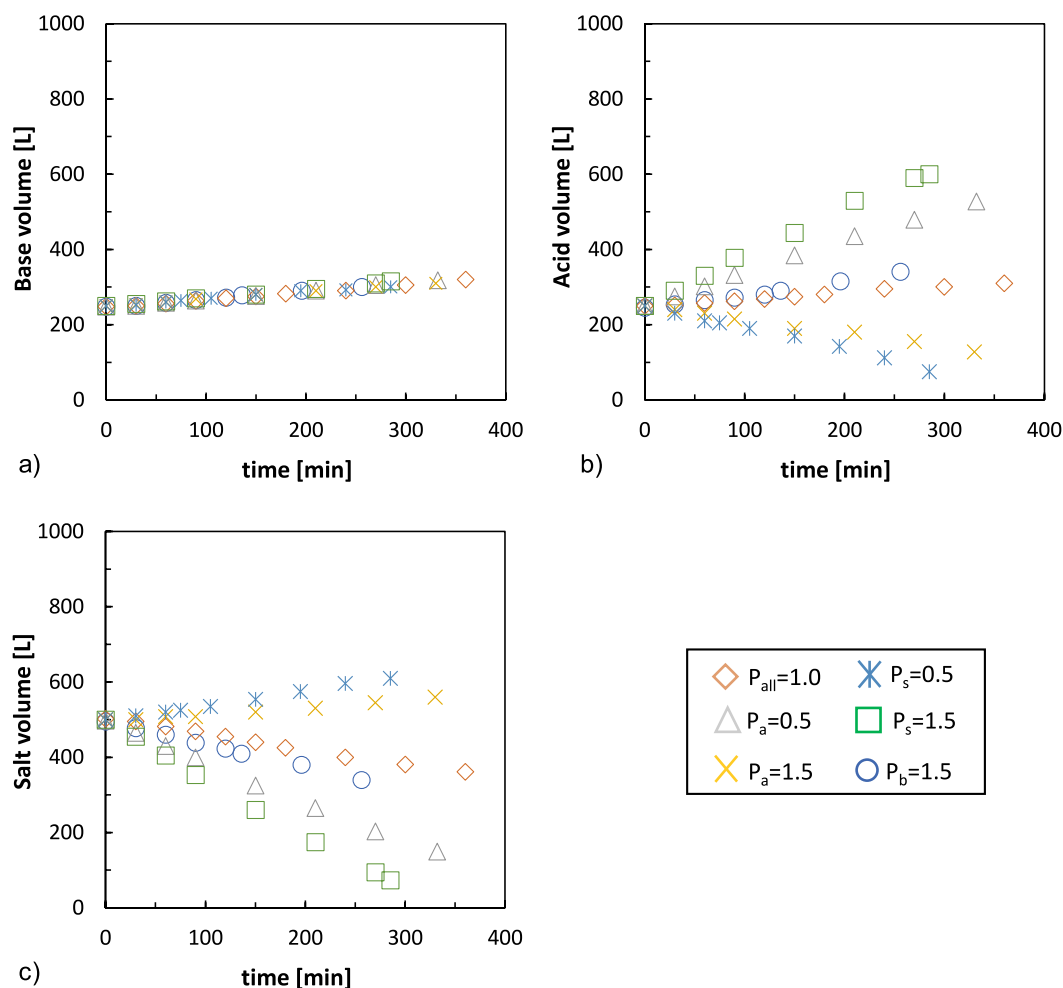
Fig. 3. a) Base, b) acid, and c) salt volume profiles as functions of time for all the investigated process conditions.

electro-osmotic flows cannot be entirely responsible for the volume variation observed after the application of pressure gradients in this work.

Considering the scenarios $P_a = 1.5$ and $P_s = 0.5$ or $P_a = 0.5$ and $P_s = 1.5$, the volume profiles had different slopes, with the acid volume profile decreasing in the first scenario and increasing in the second scenario. In particular, compared to the reference scenario ($P_{all} = 1$), the solution volume in the acid compartment nearly doubled in scenario $P_s = 1.5$ and more than halved in scenarios $P_a = 1.5$. Unlike the diffusion mechanism underlying osmotic phenomena, the hydraulic flow resulting from differential pressures between channels follows a convective transport mechanism. In other words, solution flow through either micropores (microchannels) or macropores (macrochannels) due to membrane deformation or poor gasket sealing, is driven exclusively by hydraulic pressure.

It is likely that these micropores or other pathways for solution passage are predominantly present on the anionic membrane and between the acid and salt channels. This would explain the minimal effect of differential pressure on the volume trend of the alkaline solution.

The leakage tests with softened water demonstrated that the extent of internal leakage was significantly lower under the same pressure conditions as the investigated scenarios (see Table 2). In other words, the passage of electric current or the presence of acidic/alkaline solutions somehow affects the sealing systems of the stack, the hydraulic sealing of the membranes or the nature of the pores. It is crucial to highlight this point because leakage tests are generally conducted with only water in open-loop or closed-loop configurations and equal pressures.

Fig. 4 reports the concentrations profiles for acid and base solutions and the salt conductivity as functions of time for all tests performed at different channel pressures.

In all tests, regardless of the scenario, acid and base concentrations showed an increasing trend, starting with a roughly constant slope and curving towards a plateau by the end of the tests. The final concentration values of H^+ and OH^- varied depending on the scenario, ranging between 0.53 and 1.04 mol L^{-1}. Similarly to the volume profiles, the concentration profiles of the acid and salt solutions exhibited more significant variations compared to that of the base solution, thus confirming minimal solution transport between the acid or salt and the base channels (see Fig. 4 a) and b)). Regarding the interaction between salt and acid, the H^+ concentration in the acid compartment reached 0.85 mol L^{-1} in the reference scenario. However, in the scenario with $P_a = 0.5$ or $P_s = 1.5$, it averaged 0.58 mol L^{-1}, as the greater pressure in the salt channels caused an outflow of solution towards the acid compartment, diluting the acid and reducing its concentration. In contrast, in scenarios with $P_a = 1.5$ or $P_s = 0.5$ the H^+ concentration was significantly higher, averaging 1.01 mol L^{-1}, due to the increased pressure in the acid compartment, which led to an outflow towards the salt compartment, reducing the acid volume and increasing its concentration. These shifts in solution flow between the acid and salt compartments also resulted in notable changes in the conductivity of the salt solution, influenced by the presence and relative proportions of Na^+, Cl^-, and H^+. The presence of H^+ in the salt solution is due to the greater transport of protons across the AEM from the acid compartment to the salt compartment compared
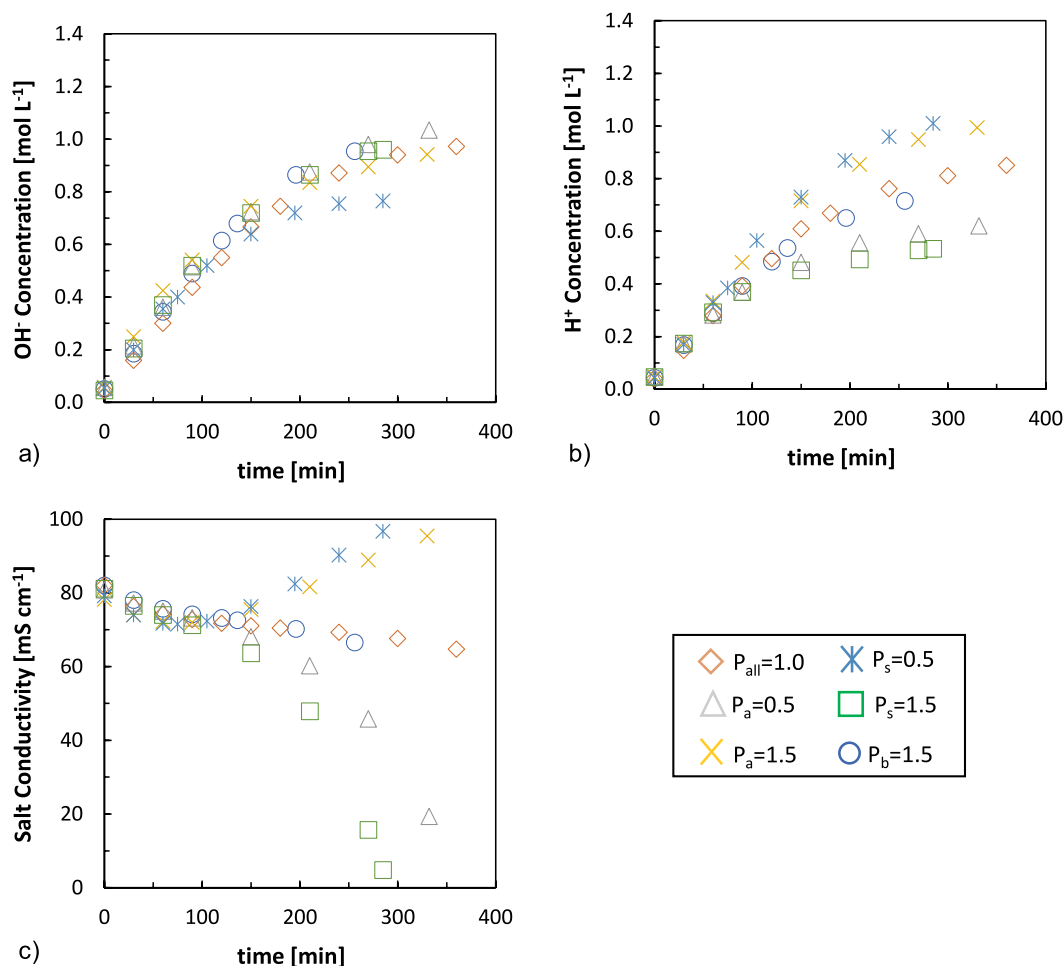
Fig. 4. a) Hydroxide ions and b) protons concentrations of the base and acid solutions, respectively, and c) salt solution conductivity as functions of time for all the investigated process conditions.

to the transport of OH^- ions across the CEM, consistent with observations in previous studies (Filingeri et al., 2023a).

The large variability in conductivity shown in Fig. 4c is associated with the hydraulic flux driven by the pressure difference across the AEM. When the conductivity increases, the direction of this flow is from the acid channel to the salt channel. On the other hand, the decrease in conductivity of the saline solution is due to the reduction in its volume over time. In this case, with the same applied current density and with 1.5 barg in the saline channel or 0.5 barg in the acid channel, the migrative flux is supported by the more rapid reduction in saline ion concentration, which ultimately leads to a rapid fall in conductivity. Therefore, in scenarios with acid pressure at 0.5 barg or salt at 1.5 barg, salt depletion is very fast, reaching conductivity values of a few mS cm^{-1}. This fact is of considerable industrial importance, as the desalination of the salt compartment significantly increases the specific energy consumption and limits the acid and base production. It is evident that the concentration values in the acid and base compartments are influenced by specific operational factors, including the configuration, the initial volume used, the current density, and the solution concentration, among others. Despite these influences, it is still possible to compare the values obtained in this study with those reported in the previous literature.

The results are in alignment with those of previous studies. For example, Cassaro et al. (2023) used a Fumatech EDBM unit with a total area of 19.2 m^2, and concentrations of up to 1.0 mol L^{-1} were achieved in closed-loop configuration. For that work, a fixed current density equal to 200 Am^{-2} was used, as well as initial volumes of 0.3 m^3 for acid and base

and 0.9 m^3 for the salt compartment. Similarly, in other studies (Virruso et al., 2024; Culcasi et al., 2022b), simulations have shown that concentrations of 1.0 mol L^{-1} can be reached in both closed-loop and feed and bleed configurations, with current densities ranging from 300 to 500 A m^{-2}.

The acid and base concentrations achieved in this work and in the available literature are demonstrably lower than those obtained using conventional industrial technologies. However, it is important to highlight that concentrated acid and base solutions are often diluted prior to use, which consumes water and wastes energy. For example, in the recovery of magnesium hydroxide from waste bitterns produced by saltworks, the employed sodium hydroxide solutions have concentrations ranging from 0.5 to 1.0 mol L^{-1} (León et al., 2022). For such applications, EDBM technology has considerable potential for the in-situ production of reagents at the desired concentrations; indeed, using EDBM in this way avoids the hazardous process of transporting, handling, and diluting concentrated reagents.

Another important aspect is the number of moles of acid and base produced over time as they are a direct measure of the EDBM productivity. These can be easily calculated from the product of the solution volume and species concentration, and the results are reported in Supplementary Material.

3.2. Effect of differential pressures on hydraulic fluxes and apparent permeability

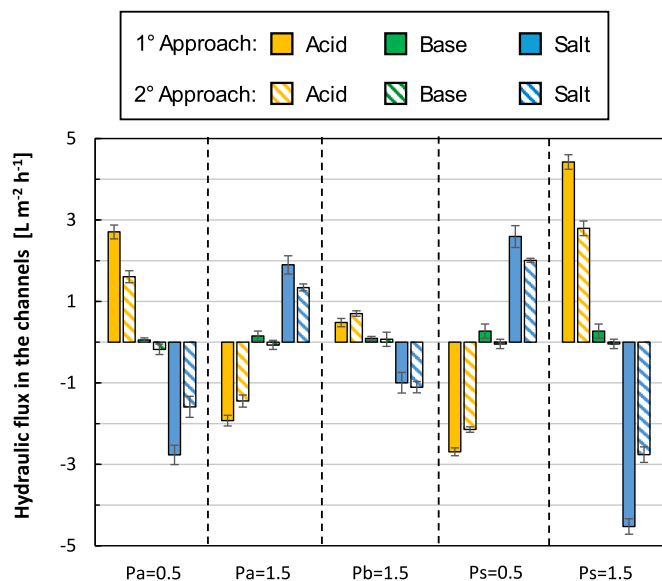In the following discussion, we aim to quantify the apparent

Fig. 5. Hydraulic flux in the three channels for all the investigated operating conditions. The two approaches to estimate hydraulic flux are described in Section 2.5.

hydraulic solution flux driven by the pressure gradient between channels. Specifically, the two different approaches, described in Section 2.5, will be used. Fig. 5 illustrates the solution fluxes calculated using these two methods across all explored scenarios.

First, we verified that the hydraulic flux was null in the reference case (with unitary pressures in the three compartments of the EDBM). In the first approach, the reference hydraulic flux is clearly zero, as it is calculated relative to the reference test itself. For the second approach, the hydraulic flux (Equation (2) at $P_{all} = 1$ is negligible (even if not zero) since the volume profile estimated using the PHREEQC software is similar to that observed experimentally (see Fig. S3 in the Supplementary Material).

The results obtained when applying the differential hydraulic pressure showed that in the alkaline compartment such hydraulic fluxes are of little significance compared to the acid and salt channels since the

average flux values (from or to the base compartment) were around 0.3 L m^{-2} h^{-1} for the first approach and -0.2 L m^{-2} h^{-1} for the second approach. This fact is due to the negligible influence of pressure variations in the base compartment on volume trends. The unit behaviour differs for the acidic and saline hydraulic solution flows, which reach maximum values of nearly 4.4 L m^{-2} h^{-1} in absolute terms under the scenario $P_s = 1.5$. Notably, the two methods used for calculating this hydraulic solution flow yield very similar results, thus confirming its convective nature. When assuming a linear relationship between the hydraulic solution flow and the applied hydraulic pressure difference between adjacent channels (see Equation (6)), it is possible to calculate the apparent hydraulic permeability of AEM and CEM to such flow, assuming the absence of this flux across the bipolar membrane. The hydraulic permeabilities for the acidic or saline channels are shown in Fig. 6 for each investigated scenario.

Fig. 6 shows that, with minimum hydraulic permeability values observed in the scenario with 1.5 in the base compartment and an average minimum hydraulic permeability of 1.5 L m^{-2} h^{-1} bar^{-1} with the solution flow occurring across the CEM. The maximum hydraulic permeabilities are seen in the scenario with $P_s = 1.5$, averaging 7.2 L m^{-2} h^{-1} bar^{-1}. As observed in Fig. 6, the permeability trends are qualitatively similar using the two different approaches for calculating this flux.

To illustrate the impact of the hydraulic flux due to differential pressures, we compared it to the flux derived from osmotic and electro-osmotic phenomena. Specifically, the hydraulic flux ranged from 7 to 12 %, which includes contributions from osmotic, electro-osmotic, and hydraulic pressure-driven phenomena, in the test at Pb = 1.5. Conversely, this flux accounted for up to 94% of the total flux when altering the acid or salt solution pressures.

This fact is also evident in terms of permeability. Specifically, the hydraulic permeability (1.5–8.8 L m^{-2} h^{-1} bar^{-1}) is approximately three orders of magnitude greater than the osmotic permeability (6.3–7.8 mL m^{-2} h^{-1} bar^{-1}).

3.3. Analysis of acid and base product purities and key performance indicators

Furthermore, the solution flux due to the application of differential pressure includes water and dissolved ions, which may alter the product purities. Fig. 7 shows the acid and alkaline product purities in all
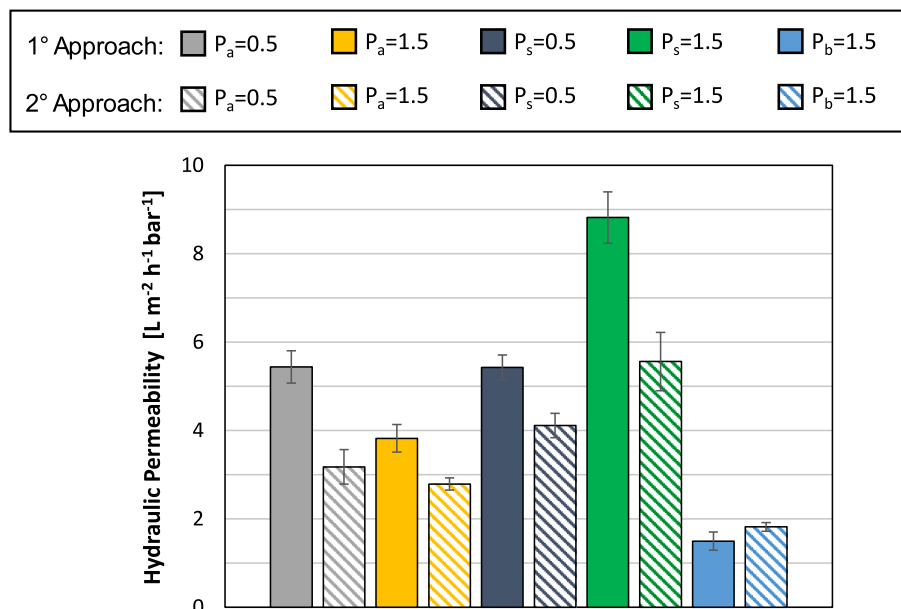

Fig. 6. Hydraulic Permeability for all the investigated operating conditions. The two approaches used to estimate the hydraulic flux are described in Section 2.5.
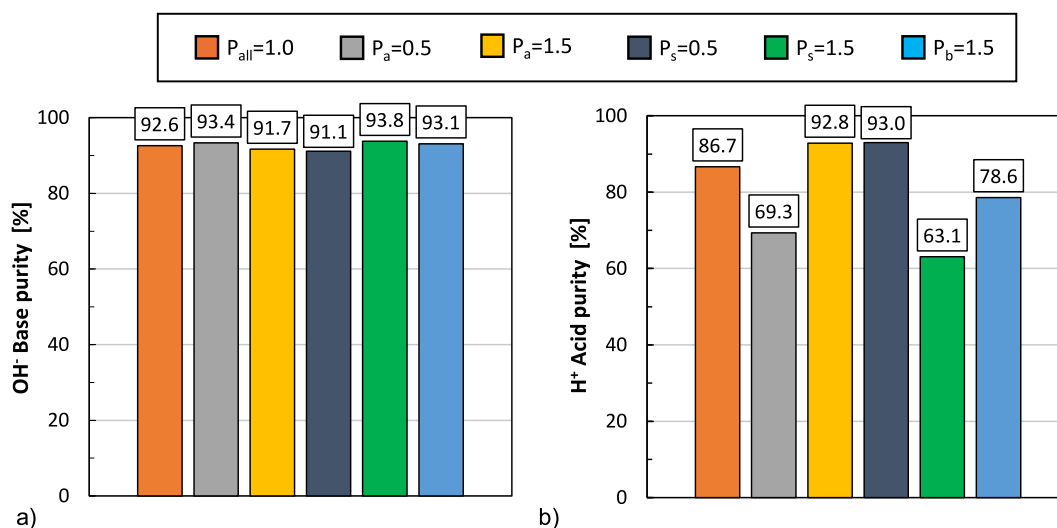
Fig. 7. a) OH⁻ Base purity and b) H⁺ Acid purity for all investigated process conditions at the end of the tests.

investigated scenarios at the end of the test. Base purity (graph a) was calculated as the ratio between the concentration of OH⁻ to the overall concentration of the anions. Acid purity (graph b) was calculated as the ratio between the concentration of H⁺ to the overall concentration of the cations.

The passage of saline solution into the acidic channel increases the concentration of Na⁺ and Cl⁻ ions in scenarios $P_a = 0.5$ and $P_s = 1.5$, thereby reducing the purity of the acid product. Conversely, the alkaline solution, not subject to such flux, does not show significant variations in purity. These results are consistent with the purities reported in the literature. For example, in a previous work (Du et al., 2021), the authors reported acid and base concentrations of 0.6 mol L⁻¹ and 0.7 mol L⁻¹, respectively, with approximately 8% impurity in the acid and 3% in the base. In a previous laboratory-scale study (Filingeri et al., 2023a) that used closed-loop configuration at 300 A m⁻², the chloride impurities in the base were found to range from 5.9% to 8.9% depending on the saline solution concentration.

Fig. 8 shows the current efficiency and the molar flux of NaOH for all studied scenarios once a specific target of 187.5 produced moles of NaOH is reached, corresponding to a OH⁻ concentrations within the range of 0.65–0.67 mol L⁻¹.

The current efficiency ranged from 64% to 86%, depending on the scenario (graph a). The highest current efficiency is observed with $P_a = 1.5$. In this case, the acid solution flow into the salt compartment leads to

a dilution effect in the acid solution, thus resulting in lower proton diffusion and less acid-base neutralization. This fact directly correlates with higher NaOH production, as shown in Fig. 8b. It is important to note that varying the scenario (and thus the applied differential pressure) significantly changes the NaOH and HCl production flux. For a given product target (i.e., the number of produced moles), lower productivity of acid and base necessitates more installed membrane area. Additionally, the current efficiency influences the SEC. Fig. 9 shows the total SEC (including both electric and pumping contribution) as the scenario varies for a fixed target (187.5 number of produced moles of NaOH).

Generally, SEC is influenced by two main factors: the electric potential and the current efficiency. As shown in Fig. 9, the SEC is highest in the scenario with $P_s = 0.5$ and lowest in the scenario with $P_a = 1.5$. In both scenarios, the predominant factor is the current efficiency, which has the lowest and highest values, respectively, among all the investigated scenarios. The scenario with $P_a = 1.5$ remained the best operating condition to achieve a lower total SEC also for a target of 125 mol (corresponding to concentrations of 0.47–0.48 mol L⁻¹) with a minimum value of 1.0 kWh kg⁻¹. This value is the lowest achieved in the previous literature with a semi-industrial scale pilot EDBM unit (see Fig. S4 in the Supplementary Material).

However, the overall system SEC is the sum of the SEC related to the EDBM unit and the energy spent on pumping the electrolyte solutions
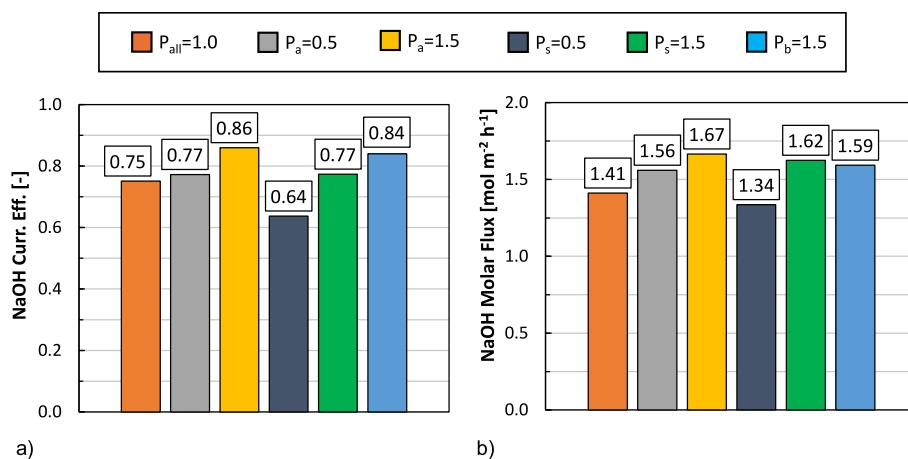

Fig. 8. a) NaOH Current Efficiency and b) NaOH Molar Flux calculated at the target of 187.5 mol of OH⁻ produced for all investigated process conditions.
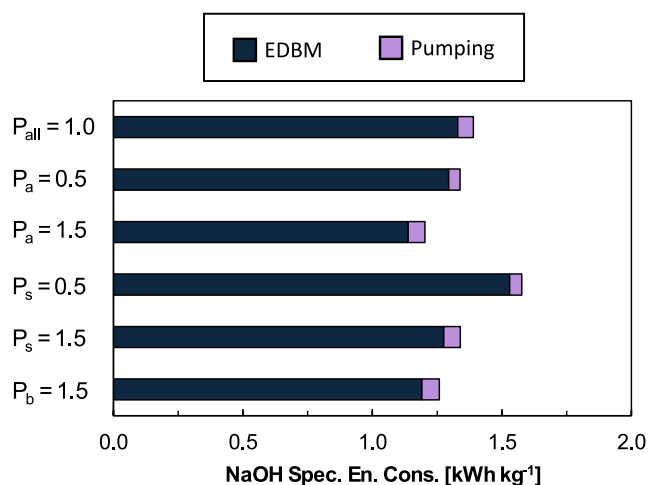
Fig. 9. EDBM and pumping Specific Energy Consumption referred to NaOH at the target of 187.5 mol of OH$^-$ produced for all investigated process the conditions.

(Equations (9)–(11)). The SEC associated with pumping varies between 0.04 and 0.07 kWh kg^{-1} and these energy consumptions do not alter the qualitative total SEC trend as the scenario changes. Therefore, the scenarios of minimum and maximum total SEC remain the same as those of EDBM SEC, with minimum value of 1.20 kWh kg^{-1} and maximum of 1.58 kWh kg^{-1} at produced moles of 187.5 in the alkaline channel with purities above 92%. As a result, the different pumping levels in the investigated scenarios do not significantly change the total SEC and, on average, the SEC for pumps accounts for 4.3% of the total, while the EDBM SEC is significantly altered.

Moreover, when targeting only 125 mol of NaOH, the minimum SEC$_{EDBM}$ value obtained was 0.94 kWh kg^{-1} in the P$_a$ = 1.5 operating scenario.

In a previous work (Filingeri et al., 2024) the performance of EDBM units equipped with Fumatech versus WTS membranes was compared in a closed-loop configuration at 300 A m^{-2}. The CE values were in the range of 76–80% for Fumatech and 71–79% for WTS membranes, which are lower than the values obtained in the present work. Conversely, the SEC values were in the range of 1.23–1.73 kWh kg^{-1} for the two types of membranes. In another study conducted at the pilot scale, the Fumatech stack achieved a CE of 80% and a SEC of 1.38 kWh kg^{-1} in closed-loop configuration at 200 A m^{-2} (Cassaro et al., 2023). Overall, the results of the present work are in line with or better than those already available in
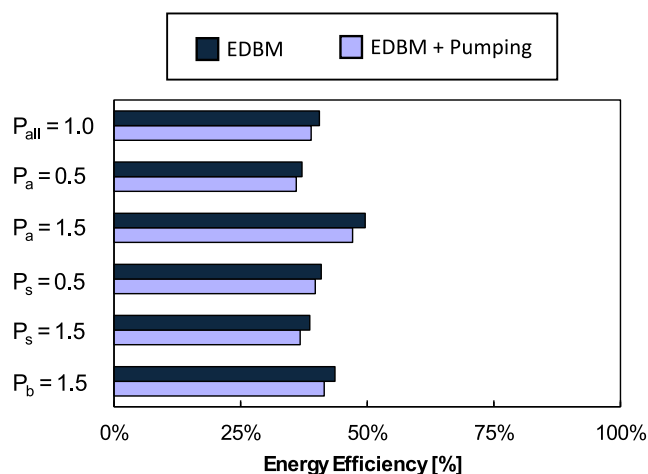
the literature, highlighting the potential of the EDBM technology.

Fig. 10 shows the energy efficiency of the EDBM unit compared to the total energy efficiency obtained when considering the pumping energy contribution (see Section 2.5) for all the investigated scenarios.

Fig. 10 indicates that the process efficiency ranged from a minimum of 37% to a maximum of 50% across all the scenarios. Although there is no reported EDBM process efficiency values in the previous literature, it is worth noting that the efficiency values align with those of conventional electrodialysis processes for water desalination (Patel et al., 2020).

Energy efficiency cannot reach 100% due to energetic losses caused by non-ideal phenomena, which also reduce the current efficiency, and ohmic losses, which lead to energy dissipation as heat (i.e., the Joule effect). Interestingly, the EDBM energy efficiency was highest in the scenario with the lowest SEC and the maximum current efficiency.

Fig. 10 also highlights the contribution made by pressure drops (i.e., the power used for pumping the electrolyte solutions) to the efficiency loss. It is notable that, according to the estimates, the efficiency loss due to pumping averaged 1.4%, thus meaning it had a minimal impact on the total energy efficiency, regardless of the pressure applied between compartments.

The performance obtained in terms of SEC and CE in this work is even better than that observed in previous studies carried out at the laboratory scale (Filingeri et al., 2024). However, the hydraulic flows induced by applying differential pressures between channels result in variations in product purity. Therefore, operating pressures should be appropriately chosen not only to reduce energy consumption but also considering the specific application and the required purity for the process.

4. Conclusions

This study presents an experimental campaign on a semi-industrial scale Electrodialysis with Bipolar Membranes (EDBM) unit, with the largest installed area ever tested and presented in the literature. Specifically, the effects of applying differential pressures across EDBM compartments were examined. The EDBM tests, conducted in a closed-loop configuration, revealed that applying a differential pressure induced a hydraulic flow of solution primarily through the anionic membrane and, to a lesser extent, through the cationic membrane. Moreover, results suggest that this hydraulic flow might be negligible across bipolar membranes, as it is driven by convective transport rather than osmotic and electro-osmotic phenomena. It might be primarily caused by micro or macro holes in the membranes or gaps formed between membranes and spacers of the EDBM stack. These phenomena, which are barely investigated in the literature, may significantly affect the performance of the EDBM unit. Particularly, operating the EDBM with a higher pressure in the acid compartment (i.e., at 1.5 barg) resulted in the lowest specific energy consumption (SEC) among the tested scenarios at a value of 1.2 kWh kg^{-1} as well as a current efficiency of 86% at 187.5 produced mols in the base channel. However, this pressure-driven flow altered the purity of the resultant products, with purity levels of 91–94% and 63–93% achieved in the base and acid compartments, respectively. The analyses showed that the average acid or salt solution flux driven by the pressure gradient between channels represented up to 94% and up to 53% of the overall volume variation for acid and salt, respectively.

It is worth noting that at the operating pressures used in this study, the average velocity in the channels ranged from 4 cm s^{-1} to 9 cm s^{-1}. Additionally, the velocity was not uniform across the three channels, even when the pressure was equal in all compartments. Generally, EDBM is operated at equal average channel flow velocities; however, this may not lead to good EDBM performance. Indeed, differential pressures can cause hydraulic flows, as demonstrated in this work, leading to performance degradation or improvements.

These findings highlight the importance of this phenomenon for

Fig. 10. EDBM and total energy efficiency referred to NaOH at the target of 187.5 mol of OH$^-$ produced for all the investigated process conditions.

EDBM operation, particularly at the industrial scale where the operating pressure is a critical variable strongly dependent on the design of the hydraulic circuits.

Post-production inspections of ion-exchange membranes conducted by the manufacturer could help clarify this phenomenon. Additionally, standardized and optimized methods for stack assembly could reduce the likelihood of gaps occurring between the membranes and spacers.

Overall, proper management of this phenomenon can significantly reduce the energy consumption and contribute to EDBM process intensification. Additionally, improving the performance of EDBM will enhance resource recovery, especially when EDBM is integrated into circular treatment systems.

CRediT authorship contribution statement

Antonia Filingeri: Writing – review & editing, Writing – original draft, Visualization, Validation, Methodology, Investigation, Formal analysis, Data curation, Conceptualization. **Andrea Culcasi:** Writing – review & editing, Writing – original draft, Visualization, Validation, Methodology, Investigation, Formal analysis, Data curation, Conceptualization. **Marcantonio Nanfara:** Visualization, Methodology, Investigation, Formal analysis, Data curation. **Calogero Cassaro:** Visualization, Methodology, Investigation, Formal analysis, Data curation. **Alessandro Tamburini:** Writing – review & editing, Supervision, Project administration, Funding acquisition. **Giorgio Micale:** Writing – review & editing, Supervision, Project administration, Funding acquisition. **Andrea Cipollina:** Writing – review & editing, Supervision, Resources, Project administration, Funding acquisition, Conceptualization.

Declaration of competing interest

The authors declare that they have no known competing financial interests or personal relationships that could have appeared to influence the work reported in this paper.

Acknowledgements

Appendix A. Supplementary data

Supplementary data to this article can be found online at https://doi.org/10.1016/j.jenvman.2024.123538.

Nomenclature

Acronyms	
AEM	Anion Exchange Membrane
BPM	Bipolar Membrane
CAPEX	Capital Expenditures
CEM	Cation Exchange Membrane
CRM	Critical raw material
DC	Direct Current
ED	Electrodialysis
EDBM	Electrodialysis with Bipolar Membranes
ERS	Electrode rinse solution
MLD	Minimum Liquid Discharge
OPEX	Operating Expenditures
PI	Purpose-designed Proportional-Integral
RED	Reverse Electrodialysis
RO	Reverse Osmosis
ZLD	Zero Liquid Discharge
Symbols	
A_m	Active membrane surface [m^2]
C	Solution concentration [$mol\ L^{-1}$]
CE	Current efficiency [%]
E_{Nernst}	Electric Nernst potential [V]
F	Faraday constant [$C\ mol^{-1}$]
GED_{EDBM}	EDBM Gross Energy Density [$kWh\ m^{-3}$]
GED_{th}	Theoretical Gross Energy Density [$kWh\ m^{-3}$]
I	Current [A]
J_{hydr}	Hydraulic flux [$L\ m^{-2}·h^{-1}$]
J_i	Ion flux [$mol\ m^{-2}\ s^{-1}$]
J_{sol}	Solution flux [$L\ m^{-2}·h^{-1}$]
$J_{w,eo}$	Electro-osmotic water flux [$mL\ m^{-2}·h^{-1}$]
$J_{w,\ os}$	Osmotic water flux [$mL\ m^{-2}·h^{-1}$]
J_w	Water flux [$mL\ m^{-2}·h^{-1}$]
k_w	Membrane permeability [$mL\ m^{-2}·h^{-1}·bar^{-1}$]
$k_{w,hydr}$	Hydraulic membrane permeability [$L\ m^{-2}·h^{-1}·bar^{-1}$]
M	Molecular weight [$g\ mol^{-1}$]
N	Number of triplet

(continued on next page)

(continued)

Acronyms	
n_H	Hydration number
P	Pressure [bar]
PED	Pump Energy Density [kWh m^{-3}]
Q	Flow rate [m^3 s^{-1}]
R	Gas constant [bar·L mol^{-1}·K^{-1}]
SEC	specific energy consumption [kWh kg$_{NaOH}^{-1}$]
T	Temperature [K]
U	Voltage [V]
V	Solution volume [L]
z	Ion valence

Greek symbols	
η_{EDBM}	EDBM energy efficiency [-]
η_p	Pump efficiency [-]
η_{total}	Total energy efficiency [-]
π	Osmotic pressure [bar]
ρ_w	Water mass density [g L^{-1}]
φ	Osmotic coefficient [-]

Subscripts and superscripts	
Acid	Acid compartment
Base	Base compartment
eo	Electro-osmotic
i	Generic ion
Initial	Initial time
Int	Interlayer
os	Osmotic
Pump	Pumping
Salt	Salt compartment
Sol	Solution
t	Generic time
target	Target
tot	Total
w	Water
0	Beginning of the test

Data availability

Data will be made available on request.

References

Adiba, N., Wang, X., Chang, C., Xu, X., Liu, Y., Ji, C., Wang, Q., Ren, Y., Wang, J., Liu, Z., Ma, Z., Gao, J., 2024. Multi-stage membrane integrated system to achieving low-mixed-salt-discharge of high-salinity mining wastewater: system design and experimental validation. Chem. Eng. Res. Des. 202, 12–22. https://doi.org/10.1016/j.cherd.2023.12.015.

An, W., Zhao, J., Lu, J., Han, Y., Li, D., 2022. Zero-liquid discharge technologies for desulfurization wastewater: a review. J. Environ. Manag. 321. https://doi.org/10.1016/j.jenvman.2022.115953.

Ankoliya, D., Mudgal, A., Sinha, M.K., Davies, P., Park, K., Alegre, R.R., Patel, V., Patel, J., 2023. Techno-economic analysis of integrated bipolar membrane electrodialysis and batch reverse osmosis for water and chemical recovery from dairy wastewater. J. Clean. Prod. 420. https://doi.org/10.1016/j.jclepro.2023.138264.

Bello, A.S., Zouari, N., Da, D.A., Hahladakis, J.N., Al-ghouti, M.A., 2021. An overview of brine management: emerging desalination technologies, life cycle assessment, and metal recovery methodologies. J. Environ. Manag. 288, 112358. https://doi.org/10.1016/j.jenvman.2021.112358.

Blengini, G.A., Latunussa, C.E.L., Eynard, U., Torres de Matos, C., Wittmer, D., Georgitzikis, K., Pavel, C., Carrara, S., Mancini, L., Unguru, M., Blagoeva, D., Mathieux, F., Pennington, D., 2020. Study on the EU's List of Critical Raw Materials (2020. Final Report. https://doi.org/10.2873/904613.

Brinkmann, T., Giner Santonja, G., Schorcht, F., Roudier, S., Delgado Sancho, L., 2014. Best available techniques reference document for the production of chlor-alkali. https://doi.org/10.2791/13138.

Cassaro, C., Virruso, G., Culcasi, A., Cipollina, A., Tamburini, A., Micale, G., 2023. Electrodialysis with bipolar membranes for the sustainable production of chemicals from seawater brines at pilot plant scale. ACS Sustain Chem Eng 11, 2989–3000. https://doi.org/10.1021/acssuschemeng.2c06636.

Chen, X., Ruan, X., Kentish, S.E., Kevin Li, G., Xu, T., Chen, G.Q., 2021. Production of lithium hydroxide by electrodialysis with bipolar membranes. Sep. Purif. Technol. 274. https://doi.org/10.1016/j.seppur.2021.119026.

Chen, T., Bi, J., Ji, Z., Yuan, J., Zhao, Y., 2022a. Application of bipolar membrane electrodialysis for simultaneous recovery of high-value acid/alkali from saline wastewater: an in-depth review. Water Res. 226. https://doi.org/10.1016/j.watres.2022.119274.

Chen, T., Bi, J., Ji, Z., Yuan, J., Zhao, Y., 2022b. Application of bipolar membrane electrodialysis for simultaneous recovery of high-value acid/alkali from saline wastewater: an in-depth review. Water Res. 226. https://doi.org/10.1016/j.watres.2022.119274.

Culcasi, A., Gurreri, L., Zaffora, A., Cosenza, A., Tamburini, A., Cipollina, A., Micale, G., 2020. Ionic shortcut currents via manifolds in reverse electrodialysis stacks. Desalination 485. https://doi.org/10.1016/j.desal.2020.114450.

Culcasi, A., Gurreri, L., Micale, G., Tamburini, A., 2021. Bipolar membrane reverse electrodialysis for the sustainable recovery of energy from pH gradients of industrial wastewater: performance prediction by a validated process model. J. Environ. Manag. 287, 112319. https://doi.org/10.1016/j.jenvman.2021.112319.

Culcasi, A., Ktori, R., Pellegrino, A., Rodriguez-Pascual, M., van Loosdrecht, M.C.M., Tamburini, A., Cipollina, A., Xevgenos, D., Micale, G., 2022a. Towards sustainable production of minerals and chemicals through seawater brine treatment using Eutectic freeze crystallization and Electrodialysis with bipolar membranes. J. Clean. Prod. 368. https://doi.org/10.1016/j.jclepro.2022.133143.

Culcasi, A., Gurreri, L., Cipollina, A., Tamburini, A., Micale, G., 2022b. A comprehensive multi-scale model for bipolar membrane electrodialysis (BMED). Chem. Eng. J. 437. https://doi.org/10.1016/j.cej.2022.135317.

Culcasi, A., Gurreri, L., Tamburini, A., Cipollina, A., Bogle, I.D.L., Micale, G., 2023. Improving efficiency and discharge power of acid-base flow battery via a bi-objective optimisation. J. Energy Storage 66. https://doi.org/10.1016/j.est.2023.107429.

Deng, Z., van Linden, N., Guillen, E., Spanjers, H., van Lier, J.B., 2021. Recovery and applications of ammoniacal nitrogen from nitrogen-loaded residual streams: a review. J. Environ. Manag. 295. https://doi.org/10.1016/j.jenvman.2021.113096.

Du, C., Du, J.R., Zhao, X., Cheng, F., Ali, M.E.A., Feng, X., 2021. Treatment of brackish water RO brine via bipolar membrane electrodialysis. Ind. Eng. Chem. Res. 60, 3115–3129. https://doi.org/10.1021/acs.iecr.1c00370.

Farsi, A., Kayhan, Ö., Zamfirescu, C., Dincer, I., Naterer, G.F., 2019. Azeotropic pressure swing distillation of hydrochloric-water for hydrogen production in the Cu–Cl cycle: thermodynamic and design methods. Int. J. Hydrogen Energy 44, 7969–7982. https://doi.org/10.1016/j.ijhydene.2019.01.048.

Filingeri, A., Lopez, J., Culcasi, A., Leon, T., Tamburini, A., Luis Cortina, J., Micale, G., Cipollina, A., 2023a. In-depth insights on multi-ionic transport in Electrodialysis with bipolar membrane systems. Chem. Eng. J. 468. https://doi.org/10.1016/j.cej.2023.143673.

Filingeri, A., Gurreri, L., Ciofalo, M., Cipollina, A., Tamburini, A., Micale, G., 2023b. Current distribution along electrodialysis stacks and its influence on the current-

voltage curve: behaviour from near-zero current to limiting plateau. Desalination 556. https://doi.org/10.1016/j.desal.2023.116541.

Filingeri, A., Herrero-Gonzalez, M., O'Sullivan, J., Rodriguez, J.L., Culcasi, A., Tamburini, A., Cipollina, A., Ibañez, R., Ferrari, M.C., Cortina, J.L., Micale, G., 2024. Acid/base production via bipolar membrane electrodialysis: brine feed streams to reduce fresh water consumption. Ind. Eng. Chem. Res. 63, 3198–3210. https://doi.org/10.1021/acs.iecr.3c03553.

Fu, R., Wang, H., Yan, J., Li, R., Wang, B., Jiang, C., Wang, Y., Xu, T., 2023. A cost-effective and high-efficiency online ED-BMED integrated system enables the conversion of 3.5 wt% NaCl aqueous solution into 6.20 mol/L NaOH. Chem. Eng. Sci. 270. https://doi.org/10.1016/j.ces.2023.118523.

Ghyselbrecht, K., Silva, A., Van der Bruggen, B., Boussu, K., Meesschaert, B., Pinoy, L., 2014. Desalination feasibility study of an industrial NaCl stream by bipolar membrane electrodialysis. J. Environ. Manag. 140, 69–75. https://doi.org/10.1016/j.jenvman.2014.03.009.

Herrero-Gonzalez, M., Culcasi, A., Tamburini, A., Ibañez, R., Cipollina, A., Micale, G., 2024. Techno-economic feasibility of photovoltaic solar electrodialysis with bipolar membranes. Desalination 582. https://doi.org/10.1016/j.desal.2024.117624.

Hussain, A., Yan, H., Ul Afsar, N., Jiang, C., Wang, Y., Xu, T., 2022. Multistage-batch bipolar membrane electrodialysis for base production from high-salinity wastewater. Front. Chem. Sci. Eng. 16. https://doi.org/10.1007/s11705-021-2114-2.

Hussain, A., Wang, H., Fu, R., Afsar, N.U., Wang, B., Jiang, C., Wang, Y., Xu, T., 2023. Ion transport behavior in bipolar membrane electrodialysis: role of anions. Ind. Eng. Chem. Res. 62, 698–707. https://doi.org/10.1021/acs.iecr.2c03812.

León, T., Abdullah Shah, S., López, J., Culcasi, A., Jofre, L., Cipollina, A., Cortina, J.L., Tamburini, A., Micale, G., 2022. Electrodialysis with bipolar membranes for the generation of NaOH and HCl solutions from brines: an inter-laboratory evaluation of thin and ultrathin non-woven cloth-based ion-exchange membranes. Membranes 12. https://doi.org/10.3390/membranes12121204.

León, T., Rodríguez, D., López, J., Jofre, L., Cortina, J.L., 2024. Optimizing operational parameters for highly-concentrated sodium hydroxide production via electrodialysis with bipolar membranes from concentrated brines. Sep. Purif. Technol. 347. https://doi.org/10.1016/j.seppur.2024.127637.

Lerch, P., Scheller, F., Reichelt, D.G., Menzel, K., Bruckner, T., 2024. Electricity cost and CO2 savings potential for chlor-alkali electrolysis plants: benefits of electricity price dependent demand response. Appl. Energy 355. https://doi.org/10.1016/j.apenergy.2023.122263.

Liu, Y., Sun, Y., Li, Y., Peng, Z., 2024. A closed-loop integrated process of bipolar membrane electrodialysis and resin adsorption for resource recovery from high-salinity phenolic wastewaters: salicylic acid manufacturing wastewater as a representative. Chem. Eng. J. 482. https://doi.org/10.1016/j.cej.2024.148681.

Marcus, Y., 2015. Ions in Solution and Their Solvation. Wiley. https://doi.org/10.1002/9781118892336.

Pärnamäe, V.Z.R., Mareev, S., Nikonenko, V., Melnikov, S., Sheldeshov, N., Hamelers, M. T.H.V.M., 2020. Bipolar membranes: a review on principles, latest developments, and applications. J Memb Sci, 118538.

Pärnamäe, R., Mareev, S., Nikonenko, V., Melnikov, S., Sheldeshov, N., Zabolotskii, V., Hamelers, H.V.M., Tedesco, M., 2021. Bipolar membranes: a review on principles, latest developments, and applications. J Memb Sci 617. https://doi.org/10.1016/j.memsci.2020.118538.

Patel, S.K., Qin, M., Walker, W.S., Elimelech, M., 2020. Energy efficiency of electro-driven brackish water desalination: electrodialysis significantly outperforms membrane capacitive deionization. Environ. Sci. Technol. 54, 3663–3677. https://doi.org/10.1021/acs.est.9b07482.

Pawlowski, S., Crespo, J.G., Velizarov, S., 2014. Pressure drop in reverse electrodialysis: experimental and modeling studies for stacks with variable number of cell pairs. J Memb Sci 462, 96–111. https://doi.org/10.1016/j.memsci.2014.03.020.

Peng, Z., Sun, Y., Shi, P., Wang, Y., 2022. A mathematical model of the external circuits in a bipolar membrane electrodialysis stack: leakage currents and Joule heating effect. Sep. Purif. Technol. 290. https://doi.org/10.1016/j.seppur.2022.120816.

SEArcularMINE website, (n.d.). https://searcularmine.eu/about/project-overview/.

Song, K., Chae, S.C., Bang, J.H., 2021. Separation of sodium hydroxide from post-carbonation brines by bipolar membrane electrodialysis (BMED). Chem. Eng. J. 423. https://doi.org/10.1016/j.cej.2021.130179.

Tanaka, Y., 2004a. The effect of solution leakage in an ion-exchange membrane electrodialyzer on mass transport across a membrane pair. J Memb Sci 231, 13–24. https://doi.org/10.1016/j.memsci.2003.10.018.

Tanaka, Y., 2004b. Pressure distribution, hydrodynamics, mass transport and solution leakage in an ion-exchange membrane electrodialyzer. J Memb Sci 234, 23–39. https://doi.org/10.1016/j.memsci.2004.01.008.

Tang, H., Wang, X., Zhao, X., Dong, Y., Xu, B., Wang, L., 2023. Ion migration characteristics during the bipolar membrane electrodialysis treatment of concentrated reverse osmosis brine. Desalination 561. https://doi.org/10.1016/j.desal.2023.116660.

U.S. Geological Survey, PHREEQC version 3. https://www.usgs.gov/software/phreeqc-version-3, 2017.

Veerman, J., Saakes, M., Metz, S.J., Harmsen, G.J., 2010. Electrical power from sea and river water by reverse electrodialysis: a first step from the laboratory to a real power plant. Environ. Sci. Technol. 44, 9207–9212. https://doi.org/10.1021/es1009345.

Virruso, G., Cassaro, C., Culcasi, A., Cipollina, A., Tamburini, A., Bogle, I.D.L., Micale, G. D.M., 2024. Multi-scale modelling of an electrodialysis with bipolar membranes pilot plant and economic evaluation of its potential. Desalination 583. https://doi.org/10.1016/j.desal.2024.117724.

Wang, H., Wang, Y., Yan, J., Fu, R., Wang, B., Jiang, C., Wang, Y., Xu, T., 2024. Bipolar membrane electrodialysis: a promising paradigm for caustic soda production. AIChE J. 70. https://doi.org/10.1002/aic.18260.